

A Short Introduction to Numerical Linked-Cluster Expansions

Baoming Tang, Ehsan Khatami, and Marcos Rigol

Department of Physics, Georgetown University, Washington DC, 20057, USA

Physics Department, The Pennsylvania State University, 104 Davey Laboratory, University Park, Pennsylvania 16802, USA

Abstract

We provide a pedagogical introduction to numerical linked-cluster expansions (NLCEs). We sketch the algorithm for generic Hamiltonians that only connect nearest-neighbor sites in a finite cluster with open boundary conditions. We then compare results for a specific model, the Heisenberg model, in each order of the NLCE with the ones for the finite cluster calculated directly by means of full exact diagonalization. We discuss how to reduce the computational cost of the NLCE calculations by taking into account symmetries and topologies of the linked clusters. Finally, we generalize the algorithm to the thermodynamic limit, and discuss several numerical resummation techniques that can be used to accelerate the convergence of the series.

Keywords: Linked-cluster expansions, Exact diagonalization, Spin systems, Lattice models

1. Introduction

1.1. High-temperature expansions

Calculating exact finite-temperature properties of quantum lattice models can be very challenging. One general approach to achieve that goal is to devise series expansions for the lattice model in question in the thermodynamic limit [1, 2]. A common example of these series expansions are high-temperature expansions (HTEs), in which the partition function \mathcal{Z} and other extensive properties of the system are expanded in powers of the inverse temperature $\beta = (k_B T)^{-1}$ (in what follows we set the Boltzmann constant k_B to unity). For example, consider the Ising Hamiltonian with nearest-neighbor interactions:

$$\hat{H} = -J \sum_{\langle i,j \rangle} \sigma_i \sigma_j, \quad (1)$$

where J is the strength of the interaction, $\langle \dots \rangle$ denotes nearest neighbors, and $\sigma_i (= \pm 1)$ is the Ising spin on site i . The partition function can be written as

$$\mathcal{Z} = \sum_{\{\sigma\}} e^{-\beta \hat{H}} = \sum_{\{\sigma\}} e^{\beta J \sum_{\langle i,j \rangle} \sigma_i \sigma_j}, \quad (2)$$

where the sum runs over all possible configurations of the spins. We define $K = \beta J$, which serves as a small

parameter in the expansion:

$$\mathcal{Z} = \sum_{\{\sigma\}} \prod_{\langle i,j \rangle} e^{K \sigma_i \sigma_j} = \sum_{\{\sigma\}} \prod_{\langle i,j \rangle} \sum_{l=0}^{\infty} \frac{K^l}{l!} (\sigma_i \sigma_j)^l \quad (3)$$

If we associate $(\sigma_i \sigma_j)^l$ to an l -fold bond between sites i and j , a typical term in the above expansion can be represented graphically as the lattice with various number of lines (including no line) connecting every two nearest-neighbor sites. Therefore, one can write the partition function in terms of contributions from all possible graphs, up to a certain size, that can be embedded on the lattice. (In the Ising model, the fact that $\sigma = \pm 1$ makes the calculations much easier than in quantum models such as the Heisenberg model.) The order in K that each graph contributes to is equal to the number of bonds it has (see Ref. [2] for more details on this derivation). Equation (3) implies that the series converges only at high temperatures, above or of the order of J . In what follows, we will see how this type of expansion is related to linked-cluster expansions.

1.2. Low-temperature expansions

Similar to HTEs, low-temperature expansions (LTEs) can be devised to describe properties of a system with discrete excited states close to its ground state, i.e., for

$\beta \rightarrow \infty$. In this approach, the partition function is written as

$$\mathcal{Z} = e^{-\beta E_0} \left[1 + \sum_{n \neq 0} e^{-\beta(E_n - E_0)} \right], \quad (4)$$

where E_0 (E_n) is the ground state (n^{th} excited state). If there is an energy increment, ϵ , satisfying $E_n - E_0 = m_n \epsilon$ with m_n being integer for all n , any thermodynamic property can be expressed as an expansion in powers of $e^{-\beta \epsilon}$. Then, cluster expansions similar to the ones discussed above for HTEs follow [2].

1.3. Linked-cluster expansions

The idea behind linked-cluster expansions (LCEs) [2, 3] is that for any extensive property P of a lattice model (such as the logarithm of the partition function or the internal energy) one can compute its value per lattice site $P(\mathcal{L})/N$ in the thermodynamic limit in terms of a sum over contributions from all clusters c that can be embedded on the lattice:

$$P(\mathcal{L})/N = \sum_c L(c) \times W_P(c), \quad (5)$$

where $L(c)$ is the multiplicity of c , namely, the number of ways per site in which cluster c can be embedded on the lattice, and $W_P(c)$ is the weight of that cluster for the property P . $W_P(c)$ is defined according to the inclusion-exclusion principle:

$$W_P(c) = P(c) - \sum_{s \subset c} W_P(s), \quad (6)$$

where

$$P(c) = \frac{\text{Tr} \left[\hat{P}(c) e^{-\beta \hat{H}_c} \right]}{\text{Tr} \left[e^{-\beta \hat{H}_c} \right]} \quad (7)$$

is the property calculated for the finite cluster c and the sum on s runs over all sub-clusters of c . In Eq. (7), \hat{H}_c is the Hamiltonian of cluster c . One can check that the weight of a disconnected cluster vanishes because $P(c)$ can be written as the sum of its parts (see Sec. 2.2), hence, the name linked-cluster expansions.

The convergence of the series in Eq. (5), when all the terms are considered, is guaranteed by the definition of weights in Eq. (6). In fact, by swapping the place of $P(c)$ and $W_P(c)$ in Eq. (6), one can write the property of a *finite* cluster c as the sum of its weight and the weights of its sub-clusters. Taking the thermodynamic limit $c \rightarrow \mathcal{L}$ brings one back to Eq. (5). However, in that limit, only a finite number of terms can be accounted for, and the series has to be truncated.

Because of the inclusion-exclusion principle [Eq. (6)], the weight of every cluster contains only

the contribution to the property that results from correlations that involve all the sites in the cluster, and in a unique fashion in accord with its specific geometry. At low temperature, when correlations grow beyond the size of the largest clusters considered in the series, the results show a divergent behavior (due to the missing contributions of clusters in higher orders of the expansion). In most of the two-dimensional quantum models of interest, this occurs near or at zero temperature, e.g., for the nearest-neighbor antiferromagnetic (AF) Heisenberg model on a bipartite lattice.

The clusters in the sum (5) are usually grouped together based on common characteristics to represent different orders [4, 5]. For instance, in the *site expansion*, where sites are used as building blocks to generate the clusters, the order of the expansion is determined by the number of sites of the largest clusters. All the clusters with n sites are said to belong to the n^{th} order. In LCEs, one has the freedom to devise an expansion (with a certain building block for generating the clusters in different orders) that best suits the particular model of interest. Some of these include the site, bond, or square expansions on the square lattice, and site, bond, or triangle expansions on the triangular and Kagome lattices, and so on [5].

Despite the simple form of the LCE equations above, its computational implementation can be challenging, as one has to (i) generate all the linked clusters that can be embedded on the lattice, (ii) identify their symmetries and topologies to compute multiplicities [this step dramatically reduces the computational effort as, for any given model, many different clusters have identical values of $P(c)$], (iii) identify the sub-clusters of each cluster to calculate weights, and (iv) calculate the property of each cluster and perform the sums. LCEs are computationally very demanding as the number of embedded clusters, and their sub-clusters, grow exponentially with increasing the order of the expansion. Below, we explain all those steps in the context of an example (the site expansion on a finite square lattice). We should stress that the HTE explained above for the Ising model can be seen as a LCE in which the property for each cluster is calculated using a perturbative expansion of Eq. (7) in terms of K .

1.4. Numerical linked-cluster expansions

In this work, we present a pedagogical overview of the *numerical* linked-cluster expansions (NLCEs) introduced in Ref. [4]. NLCEs use the basis of LCEs, but employ exact diagonalization (ED), instead of perturbation theory as done in HTEs, to calculate the properties of finite clusters in the series. This means that

the properties of each cluster are calculated to all orders in β . The main advantage of NLCEs over HTEs is that, for models with short-range correlations, it is possible to access arbitrarily low temperatures because of the lack of a small parameter in the series. Furthermore, for models in which correlations grow slowly as the temperature is lowered, NLCEs can converge well below the temperature at which HTEs diverge. In NLCEs, as opposed to HTEs, the convergence temperature is controlled by the correlations in the model, and by the highest order in the series that can be calculated.

The basics of NLCEs, and results for various spin and itinerant models in the square, triangular and kagome lattices, were presented in Refs. [4, 5, 6]. Recent applications of this method exploring properties of frustrated magnetic systems can be found in Refs. [7, 8, 9]. NLCE studies of the Hubbard model in the square and honeycomb lattices were reported in Refs. [10, 11, 12]. How to deal with Hamiltonians and observables that break some of the symmetries of the underlying lattice was discussed in Refs. [13, 14]. Finally, how to generalize NLCEs to calculate ground-state as well as low-temperature properties of lattice Hamiltonians with dimerized ground states was the subject of Ref. [15], while direct ground state calculations in the thermodynamic limit were done in Ref. [16] and dynamics were explored in Ref. [17].

Here, we introduce NLCEs for finite clusters, in order to show how they converge to the exact result with increasing the order in the expansion, and, later, discuss NLCEs in the thermodynamic limit. The exposition is organized as follows. In Sec. 2, we present the algorithmic details and the numerical implementation of NLCE in two dimensions for a finite 4×4 lattice. In Sec. 2.7, we report results of the expansion for the AF Heisenberg model on this cluster and compare them, in each order, to exact results that can be obtained by means of full exact diagonalization of the 4×4 lattice. In Sec. 3, we discuss how to extend NLCEs to the thermodynamic limit, and compare NLCE results for the Heisenberg model to those from large-scale quantum Monte Carlo (QMC) simulations. In Sec. 4, we describe two resummation techniques that have been found to be widely applicable to accelerate the convergence of the NLCEs for thermodynamic properties of lattice models of interest.

2. Implementation of NLCEs for Finite Systems

In this section, we sketch the NLCE algorithm for an arbitrary Hamiltonian that only connects nearest-neighbor sites on a $N = 16$ site square lattice with open boundary conditions, which is shown in Fig. 1. We have

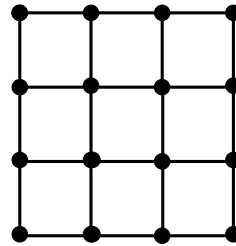


Figure 1: The 4×4 finite lattice with open boundary conditions used as an example in the derivation of the NLCE.

chosen this small lattice because it allows us to carry out the NLCE to all orders in the site expansion. It also allows us to compare the properties in each order of the expansion to exact results calculated directly by ED of the entire 16-site system.

2.1. Embedded clusters

There exists $\binom{N}{n} = \frac{N!}{n!(N-n)!}$ clusters in the n^{th} order on a lattice with N sites. To identify them in a computer, one can number the lattice sites in an arbitrary fashion. Then, construct an array of size N whose i^{th} element is a binary number representing site number i on the lattice. A 0 as an element of this array indicates that the corresponding site is not part of the generated cluster whereas a 1 indicates that it is part of the cluster. Therefore, all

Table 1: Total number of embedded clusters (second column), number of linked-clusters (third column), number of linked-clusters that are not related by point-group symmetries (fourth column), and number of linked-clusters that are topologically distinct (fifth column), in each order of the site expansion for a 16-site lattice with nearest-neighbor interactions (Fig. 1).

| n | $\frac{N!}{n!(N-n)!}$ | Connected | Sym. distinct | Topo. |
|-----|-----------------------|-----------|---------------|-------|
| 1 | 16 | 16 | 1 | 1 |
| 2 | 120 | 24 | 1 | 1 |
| 3 | 560 | 52 | 2 | 1 |
| 4 | 1820 | 113 | 5 | 3 |
| 5 | 4368 | 244 | 14 | 4 |
| 6 | 8008 | 496 | 43 | 10 |
| 7 | 11440 | 912 | 94 | 19 |
| 8 | 12870 | 1474 | 197 | 49 |
| 9 | 11440 | 2032 | 296 | 92 |
| 10 | 8008 | 2286 | 327 | 167 |
| 11 | 4368 | 2000 | 265 | 190 |
| 12 | 1820 | 1236 | 169 | 152 |
| 13 | 560 | 488 | 66 | 65 |
| 14 | 120 | 116 | 20 | 20 |
| 15 | 16 | 16 | 3 | 3 |
| 16 | 1 | 1 | 1 | 1 |

clusters in the n^{th} order can be generated by exploring all possible configurations of 1 and 0 as elements of the above array, while keeping the total number of nonzero elements fixed at n .

In the second column of Table 1, we list $\binom{N}{n}$ for our example of the 16-site lattice in Fig. 1. Once we have all the site clusters, we need to connect the sites present on them with bonds. This is done following the Hamiltonian of interest. For models with nearest-neighbor interactions, the case of interest here, bonds are added to every pair of nearest-neighbor sites [4]. Hence, each site in our clusters is connected by bonds with up to 4 other sites. Examples of clusters within the site expansion are given in Fig. 2.

2.2. Connected clusters

Many of the site clusters generated in the step above contain disconnected parts. Those clusters should be discarded because their weight $W_P(c)$, as given by Eq. (6), is zero. This can be easily seen if one assumes that cluster c consists of two disconnected sub-clusters c_1 and c_2 . Then, since $P(c)$ is extensive, it can be written as the sum of the properties of the two sub-clusters:

$$P(c) = P(c_1) + P(c_2). \quad (8)$$

But, in addition to all of their subclusters, c_1 and c_2 themselves are among the subclusters of c . Therefore,

$$\begin{aligned} W_P(c) &= P(c) - \sum_{s \subset c} W_P(s) \\ &= P(c) - \left[W_P(c_1) + \sum_{s \subset c_1} W_P(s) \right] \\ &\quad - \left[W_P(c_2) + \sum_{s \subset c_2} W_P(s) \right] \\ &= P(c) - P(c_1) - P(c_2) = 0. \end{aligned} \quad (9)$$

One then needs to find a way to distinguish between connected and disconnected clusters. A cluster is connected if starting from any site one can reach any other site moving along the bonds (only nearest-neighbor bonds in our case). We have implemented this idea by reconstructing the cluster from scratch. In our codes,

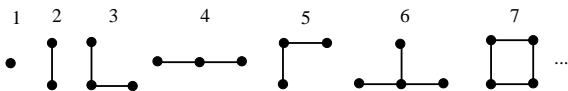


Figure 2: A sample of linked clusters that can be embedded on our finite 16-site lattice. Clusters 3 and 5 are related by point-group symmetry and are topologically the same as cluster 4.

starting from one of the sites in the cluster, we add bonds between that site and all of its neighboring sites, provided that they are part of the cluster. The same process is repeated for each of the new sites and this continues until there are no more options for adding bonds. The resulting cluster is then compared to the original one. If they are not identical, the cluster must have disconnected parts and is discarded.

In the third column in Table 1, we show the number of clusters in each order of the site expansion after the disconnected ones have been removed. Figure 2, depicts some of the linked clusters generated for our 16-site lattice.

2.3. Point-group symmetries

If the Hamiltonian preserves the symmetries of the underlying lattice, clusters related by point-group symmetries have the same weight for all observables. Therefore, they can be grouped together in order to avoid repeating the calculation of the weights for all of them. Depending on the lattice, one may have different number of point-group symmetries. For the square lattice, which is the case in our example, one has the following eight point group symmetries:

- Identity
- Reflection about $x = 0$
- Rotation by 90°
- Reflection about $y = 0$
- Rotation by 180°
- Reflection about $x = y$
- Rotation by 270°
- Reflection about $x = -y$

Hence, at this point in the implementation of the NLCEs, the goal is to identify and keep only those clusters that are not related by point-group symmetries. We achieve this through the following steps, which need to be followed independently for each order of the expansion:

- (i) Create a list of symmetrically distinct clusters and their multiplicity. This list begins with the first linked cluster in the order under consideration with multiplicity one.
- (ii) Take the next connected cluster and generate all clusters that are symmetrically related to it by applying the symmetry operations mentioned above.
- (iii) For each cluster generated in (ii), check whether it is present in the list created in (i). This is achieved by finding out whether there is a translation vector that converts one cluster into the other. If yes, increase the multiplicity of the stored cluster that is a match by one, and go to (ii).

- (iv) If none of the clusters generated in (ii) is in the list created in (i), store the connected cluster in the list, set its multiplicity to one, and go to (ii).

This step significantly reduces the number of clusters that one has to consider. Among the clusters shown in Fig. 2, clusters 3 and 5 are related by a 90° rotation and only one of them needs to be stored. The fourth column in Table 1 shows the number of clusters that are not related by point-group symmetries in each order of the site expansion.

2.4. Topological clusters

Furthermore, even if some clusters are not related by point-group symmetries, their Hamiltonian may be identical. For example, in models with only nearest-neighbor terms, clusters 3 and 4 in Fig. 2 have the same Hamiltonian. We then say that these two clusters are topologically equivalent, and only one of them needs to be diagonalized. It is important to note that topologically equivalent clusters share the same thermodynamic properties, but they may lead to different results for correlation functions. For example, the distance between the two extreme sites in clusters 3 and 4 in Fig. 2 is $2a$ and $\sqrt{2}a$ (a is the lattice spacing), respectively, and that difference needs to be taken into account when calculating correlation functions. Still, since the full exact diagonalization of each cluster is the most time consuming part of the NLCE calculations, the fact that one only needs to diagonalize topologically different clusters (or simply, *topological clusters*) reduces the computation time dramatically.

At this point, we need to generate a list of all topological clusters. It can be easily verified that they share the same topologically distinct sub-clusters, i.e., only diagonalizing topological clusters allows one to carry out the entire NLCE calculations.

The identification of the cluster topologies can be done through adjacency matrices (M). An adjacency matrix contains all the information about the spatial relations between sites in the cluster. In the simplest form, an adjacency matrix of an n -site cluster for a model with only nearest-neighbors interaction can be a $n \times n$ matrix whose rows/columns represent different sites and the matrix elements, M_{ij} , are either 1, if sites i and j are nearest neighbors (are connected by a bond), or 0 otherwise. Such matrix will be symmetric with zeros as diagonal elements. A generalized version of such matrices can be used for models with bond anisotropy or correlations beyond nearest neighbors.

If two clusters of the same size are topologically equivalent, then there exists a permutation of sites that

transforms the adjacency matrix of one onto the other. Therefore, similar to the approach taken in the previous step, we make a list of topologically distinct clusters for each order as follows:

- (i) Create a list of topological clusters and their multiplicity. This list begins with the first symmetrically distinct cluster in the order under consideration with its multiplicity.
- (ii) Take the next symmetrically distinct cluster and construct its $n!$ possible adjacency matrices (given the $n!$ site permutations).
- (iii) For each adjacency matrix generated in (ii), check whether it coincides with the adjacency matrix of any of the clusters in the list created in (i). If yes, increase the multiplicity of the stored cluster that is a match by the multiplicity of the new cluster, and go to (ii).
- (iv) If none of the adjacency matrices generated in (ii) matches the one of a cluster in the list created in (i), store the newly found topological cluster in the list, set its multiplicity to the one it had as a symmetrically distinct cluster, and go to (ii).

In practice, this part of the algorithm can be very time consuming not only because the number of permutations can be very large, but also because of the matrix comparisons. So, alternatively, one can generate a *key* (an individualized number) for each adjacency matrix and use that key for comparison purposes. To do that, one has to pick only one, out of the $n!$ adjacency matrices to represent a cluster. This can be accomplished by labeling sites according to a unique criterion for the adjacency matrix. For example, if we think of each adjacency matrix as a large binary number by attaching its columns/rows one after another, one can pick the permutation of site numbers that yields the largest (or smallest) binary number. In Fig. 3, we show one of the adjacency matrices of a four-site cluster and the same matrix after exchanging site labels 1 and 2. The latter, which yields the smallest binary number that consists of columns of the matrix, is the one that will represent this cluster and that will be stored.

The recipe for generating the keys is arbitrary and, for large cluster sizes, one may not be able to find a recipe that guarantees a unique key for each cluster, i.e., multiple adjacency matrices may end up sharing the same key. The following is an example of one such recipe for creating the keys:

$$\text{key} = \sum_{i,j} M_{ij}(i \times j)^{i+j}. \quad (10)$$

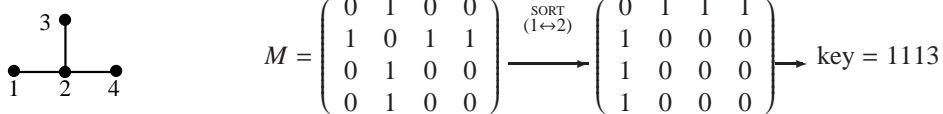


Figure 3: An example of the adjacency matrix that represents a 4-site cluster (left). Rows and columns are representatives of the sites on the cluster. A 1 (0) as the (i, j) element of the matrix indicates that sites i and j are connected (not connected) by a nearest-neighbor bond. The matrix on the right is sorted by exchanging sites 1 and 2. A key is associated to the sorted matrix according to an arbitrary formula [here, we use Eq. (10)].

If the key is not unique, then when the key of a new cluster matches the one of a stored topological cluster, one has to directly compare the adjacency matrices in order to determine whether the two clusters are topologically the same. We emphasize that the use of keys accelerates the process of comparing adjacency matrices tremendously and has been implemented in all our NLCEs.

Up to this point, we have identified and stored the topological clusters of each size, their multiplicities, and their adjacency matrices with their respective keys. The number of topological clusters in each order of our example is shown in the last column in Table. 1. This table now makes apparent the significant reduction of the number of clusters that need to be fully diagonalized from the initial $\binom{N}{n}$. In the following step, we explain how to enumerate the sub-clusters of each topological cluster to be able to ultimately calculate its weight.

We should stress that the approach described here to identify topologically distinct clusters works so long as the cluster sizes are small enough that all permutations of the introduced adjacency matrices can be explored. For larger cluster sizes, one needs to generate more sophisticated adjacency matrices whose description is beyond the scope of this introduction to NLCEs.

2.5. Sub-clusters

Given the description so far for finding topological clusters, identifying all subclusters of a topological cluster is a relatively straightforward task. Note that finding the topological clusters of our finite 16-site lattice can, in itself, be interpreted as finding all subclusters of a 4×4 cluster in the list of topological clusters of a larger lattice. Therefore, following the same procedure as in Sec. 2.1 and Sec. 2.2, and replacing the 4×4 system with any of the topological clusters, we first generate all possible connected subclusters. This time, there is no need for checking the point-group symmetries of the subclusters (Sec. 2.3). This is because all clusters that are related by symmetry share the same topology and have the same adjacency matrix. So, after generating

a new connected subcluster, it is sufficient to construct its adjacency matrix and compare it to those of clusters with the same size that are stored in the list of topological clusters. Since there will always be a match, one only needs to keep track of how many subclusters of a certain topology a topological cluster has. The latter can be achieved by considering a multiplicity matrix, Y , whose (i, j) element gives the number of times the j th topological cluster can be embedded in the i th topological cluster.

The steps described from Sec. 2.1 to Sec. 2.5 need to be carried out just once for all Hamiltonians involving only nearest-neighbor terms in the square lattice. The table with all topological clusters and subclusters can be stored and used for different nearest neighbor Hamiltonians and, for any given Hamiltonian, for different microscopic parameters.

2.6. Weights

Now, we have all the necessary tools to account for the subcluster subtractions in order to calculate the weights in Eq. (6). The steps that follow need to be carried out every time that a new Hamiltonian or Hamiltonian parameter is explored. One starts with the smallest cluster in the first order. That cluster has no subclusters and, therefore, the weight of the property P in the cluster is simply equal to the property $P(1)$. Then, to compute the weight of the next topological cluster (a single bond in the second order of our site expansion, see Fig. 2), we have to subtract the weight of the cluster in the first order from its property, according to the multiplicities given by the matrix Y :

$$\begin{aligned} W_P(1) &= P(1) \\ W_P(2) &= P(2) - Y_{21}W_P(1) = P(2) - Y_{21}P(1) \\ &\vdots \end{aligned} \tag{11}$$

In the above equations, indices 1 and 2 refer to the cluster number, c , which is not necessarily the order number. As mentioned in Sec. 1.3, in NLCEs, the property $P(c)$

is calculated using ED. For instance, the internal energy is:

$$E(c) = \langle \hat{H}_c \rangle = \frac{\sum_{n=1}^{M_c} \varepsilon_n(c) \exp[-\beta \varepsilon_n(c)]}{\sum_{n=1}^{M_c} \exp[-\beta \varepsilon_n(c)]}, \quad (12)$$

where \hat{H}_c is the Hamiltonian for the finite cluster c with eigenvalues $\varepsilon_n(c)$, and M_c is the size of the Hilbert space on that cluster.

We define partial sums, S , to group together contributions from topological clusters with a common characteristic in one order of the NLCE. For example, in the site expansion, the most natural characteristic is the number of sites. Therefore, S_n , which is the sum of the contributions to property P from all n -site topological clusters in the series (c_n) reads

$$S_n = \sum_{c_n} L(c_n) W_P(c_n). \quad (13)$$

The property in the m th order of NLCE is then

$$P_m(\mathcal{L})/N = \sum_{n=1}^m S_n. \quad (14)$$

2.7. Results for the AF Heisenberg model

Now that we have sketched the site expansion for a 16-site lattice and for generic Hamiltonians that connect only nearest-neighbor sites, let us consider a specific example of one such Hamiltonians, namely, the AF Heisenberg model

$$\hat{H} = J \sum_{\langle i,j \rangle} \hat{\mathbf{S}}_i \cdot \hat{\mathbf{S}}_j, \quad (15)$$

where $\hat{\mathbf{S}}_i$ is the spin operator at site i . For simplicity, we set $J = 1$ so that, in what follows, all energies are given in units of J .

In Fig. 4, we show results for the energy per site (a), the entropy per site (b),

$$S = \frac{1}{N} \left(\ln Z + \frac{\langle \hat{H} \rangle}{T} \right), \quad (16)$$

and the specific heat per site (c),

$$C_v = \frac{1}{N} \frac{\langle \hat{H}^2 \rangle - \langle \hat{H} \rangle^2}{T^2}, \quad (17)$$

on the 16-site lattice. The exact results (labeled ‘‘Exact’’ in Fig. 4) were obtained by means of full diagonalization of the Hamiltonian, and are compared to those obtained in different orders of the site expansion

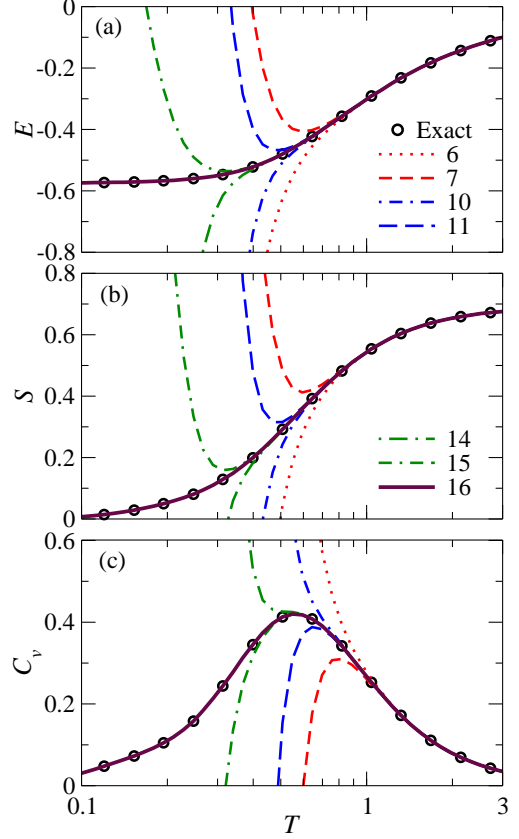


Figure 4: (a) Energy, (b) entropy, and (c) specific heat per site vs temperature for the AF Heisenberg model on the 16-site cluster in Fig. 1. Exact results are obtained by full exact diagonalization of the 16-site cluster with open boundary conditions and are compared to those in different orders of the site expansion explained throughout this work.

[Eq. (14)]. Two things are apparent in those plots: (i) with increasing order, the NLCE results converge to the exact ones at lower temperatures. (ii) At any given order, quantities that can be represented by lower order derivatives of the partition function converge to lower temperature. Note the contrast between the results for the energy and C_v . Interestingly, even in the 15th order, when only the contribution from the 16-site cluster is missing, the energy has a visible discrepancy with the exact result at temperatures as high as $T = 0.3$.

3. Thermodynamic Limit

The generalization of the NLCE presented above to the thermodynamic limit is straightforward. Only certain steps in the algorithm change when dealing with the infinite-size system. In this section, we discuss

those changes and show NLCE results for the Heisenberg model [Eq. (15)] in the thermodynamic limit.

First, for the generation of the clusters, we start with the smallest one (a site in the site expansion) and systematically add more building blocks (sites in the site expansion). Hence, to generate clusters with $n + 1$ sites, we consider all symmetrically distinct clusters that have n sites and add a nearest-neighbor site to every site at the edge of the cluster. Note that this way of building site clusters works because of translational invariance in the infinite lattice, and it is not appropriate for the finite system in Fig. 1 where not all sites are equivalent. This approach not only guarantees the generation of all possible clusters that can be embedded on the infinite lattice, but also produces only connected clusters, i.e., the step presented in Sec. 2.2 (examining the connectivity of the clusters) can be skipped. The second column in Table 2 show the number of connected clusters per site, with up to 17 sites, in the site expansion of the square lattice in the thermodynamic limit.

For finite systems without translational symmetry, all the different embeddings of a particular cluster are automatically generated in the approach discussed in Sec. 2.1. Thus, the multiplicity of a symmetrically distinct cluster is calculated by counting the times it appears in the process of generating all clusters. For the infinite system, because of translational symmetry, the multiplicity is simply equal to the number of point-group symmetries that transform a cluster to another cluster that is not related to the first one by a translation. Hence, a process similar to the one carried out for identifying the symmetries of the clusters on a finite lattice needs to be implemented for the clusters of the infinite system. However, in the latter, the multiplicity of symmetrically distinct clusters are determined immediately after building them by just examining their point-group symmetries. Moreover, if by adding sites to a cluster in the previous order one finds a new cluster that is related by a symmetry operation to one of the clusters stored in the new list, we simply dismiss it. The third column in Table 2 show the number of symmetrically distinct clusters per site, with up to 17 sites, in the site expansion of the square lattice in the thermodynamic limit.

After finding all symmetrically distinct clusters, we follow exactly the same procedure described in Secs. 2.4 and 2.5 to determine all topological clusters and their subclusters. For the site expansion in the square lattice, the last column in Table 2 show the number of topological clusters per site in the thermodynamic limit. We should stress that all the steps described above need to be carried out just once for all lattice Hamiltonians that only connect nearest-neighbor sites in the square lattice.

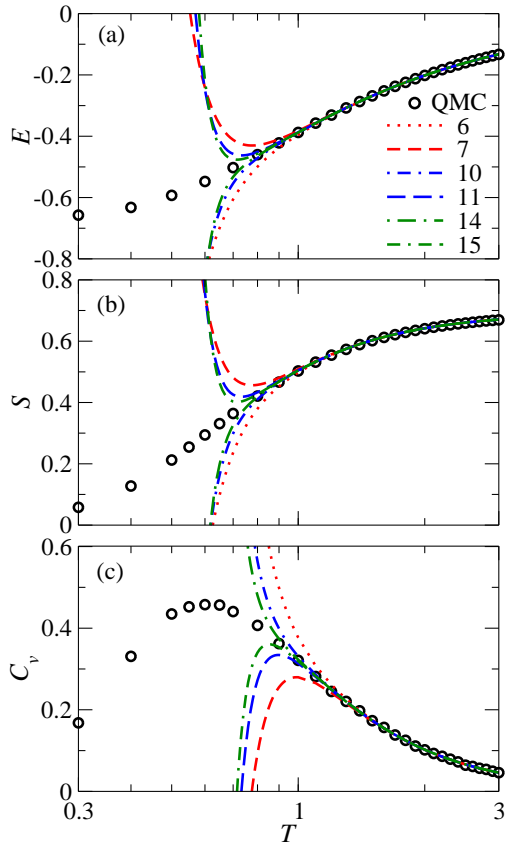


Figure 5: (a) Energy, (b) entropy, and (c) specific heat per site of the AF Heisenberg model on the square lattice in the thermodynamic limit as a function of temperature. NLCE bare sums up to 15th order are compared with QMC results for a 256×256 lattice.

Once the topological clusters and subclusters are determined, one can study any nearest-neighbor model of interest. In Fig. 5, we show results for the energy (a), the entropy (b), and the specific heat (c) per site for the AF Heisenberg model on the square lattice, and up to the 15th order of the site expansion. NLCE results are compared to those obtained by means of QMC simulations, previously reported in Ref. [13], for a very large periodic system with 256×256 sites. Those plots exhibit qualitatively similar features to the ones in Fig. 4 for a finite cluster. Namely, as the order increases, NLCE results converge to lower temperature. In addition, the energy and the entropy can be seen to converge to lower temperature than the specific heat. We note that, only in the 15th order, there are 42,192 topological clusters that need to be diagonalized (see Table 2). Because of the very large number of clusters, one can use an embarrassingly parallel code that distributes groups of clusters to different processors so that one diagonalizes many of

them at once in every order of the NLCEs.

4. Resummation Algorithms

As seen from the results in Fig. 5, the bare sums of the NLCE convergence down to a temperature that depends on the order up to which the expansion can be carried out and, on a more fundamental level, it depends on the build up of correlations in the system as the temperature is lowered. The longer the correlations the larger the cluster sizes that need to be included in the series to achieve convergence. Fortunately, even if one cannot calculate more orders of the NLCE, because of the exponential increase of the number of clusters and of the Hilbert space of each cluster, several numerical resummation algorithms have been developed that accelerate the convergence of NLCEs [5].

The goal of those algorithms is to estimate $P(\mathcal{L})/N = \lim_{m \rightarrow \infty} P_m$ in Eq. (14) from a finite set $\{P_m\}$. Resummation techniques then provide results for the observables of interest in regions where the bare sums [Eq. (14)] do not converge. Here we will focus our discussion on two such methods: Wynn's algorithm [18] and Euler's transformation [19]. They have been shown to be extremely useful in accelerating the convergence of NLCEs for thermodynamic properties in several models of

Table 2: Total number of linked-clusters (second column), number of linked-clusters that are not related by point-group symmetries (third column), and number of linked-clusters that are topologically distinct (fourth column) per site, up to the 17th order of the site expansion of the square lattice (in the thermodynamic limit) with nearest-neighbor interactions.

| n | Connected | Sym. distinct | Topo. |
|-----|-----------|---------------|--------|
| 1 | 1 | 1 | 1 |
| 2 | 2 | 1 | 1 |
| 3 | 6 | 2 | 1 |
| 4 | 19 | 5 | 3 |
| 5 | 63 | 12 | 4 |
| 6 | 216 | 35 | 10 |
| 7 | 760 | 108 | 19 |
| 8 | 2725 | 369 | 51 |
| 9 | 9910 | 1285 | 112 |
| 10 | 36446 | 4655 | 300 |
| 11 | 135268 | 17073 | 746 |
| 12 | 505861 | 63600 | 2042 |
| 13 | 1903890 | 238591 | 5450 |
| 14 | 7204874 | 901971 | 15197 |
| 15 | 27394666 | 3426576 | 42192 |
| 16 | 104592937 | 13079255 | 119561 |
| 17 | 400795844 | 50107909 | 339594 |

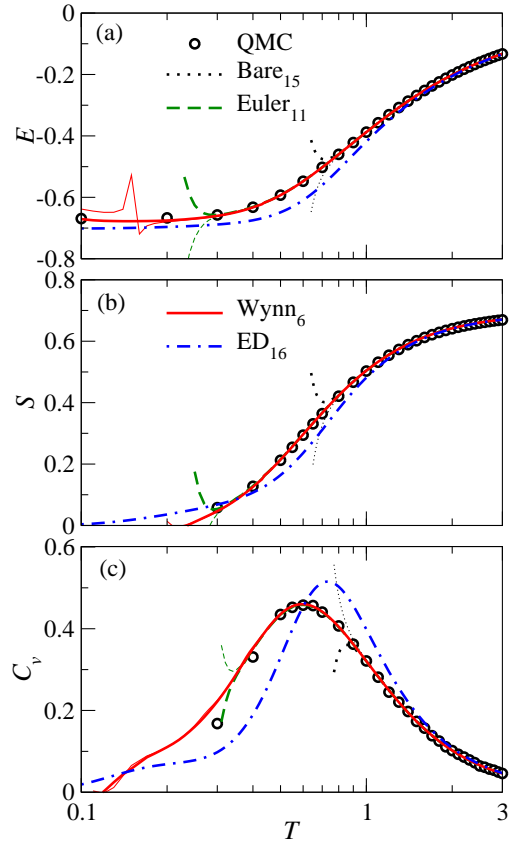


Figure 6: (a) Energy, (b) entropy, and (c) specific heat per site of the AF Heisenberg model on the square lattice as a function of temperature. Here we show results of last two orders (thick lines are used for the last order and thin lines for the one to last order) for the NLCE bare sums (up to the 15th order), Wynn's algorithm with 6 cycles of improvement, and Euler's transformation (for the last 11 orders). Results from a large-scale QMC and exact diagonalization of a 16-site cluster with periodic boundary conditions are also shown.

interest [4, 5, 6, 10, 11, 12, 13, 14, 15].

In Wynn's algorithm, one defines

$$\begin{aligned} \varepsilon_n^{(-1)} &= 0, \quad \varepsilon_n^{(0)} = P_n, \\ \varepsilon_n^{(k)} &= \varepsilon_{n+1}^{(k-2)} + \frac{1}{\Delta \varepsilon_n^{(k-1)}}, \end{aligned} \quad (18)$$

where the differentiating operator Δ is applied to subscripts and is expressed as

$$\Delta \varepsilon_n^{(k-1)} = \varepsilon_{n+1}^{(k-1)} - \varepsilon_n^{(k-1)}. \quad (19)$$

It is expected that the even entries $\varepsilon_n^{(2l)}$ converge to $P(\mathcal{L})/N$, while the odd ones $\varepsilon_n^{(2l+1)}$ usually diverge, where l is defined as the number of cycles of improvement. As an example, assume that the highest order in the NLCE that can be considered is m , i.e., the bare sum yields P_m for the property in the last order. Now, assume

that we use the Wynn algorithm with $l = 1$ (one cycle of improvement) instead. In that case,

$$P_m \rightarrow \varepsilon_{m-2}^{(2)} = P_m - \frac{S_m}{1 - \frac{S_{m-1}}{S_m}}, \quad (20)$$

where the second term in the right hand side is the first order correction to the result of the bare sum. Yet, it can often significantly improve the convergence. Note that, for every cycle of improvement, there will be two terms less in the new series determined by means of Eq. (18) ($P_m \rightarrow \varepsilon_{m-2l}^{(2l)}$).

We have found that this algorithm is one of the best for accelerating the convergence of NLCEs. In Fig. 6(a), we show the same energy as in Fig. 5(a) but include the results obtained after six cycles of improvement using Wynn's algorithm. One can see that the last two orders of the Wynn sum (red solid lines) agree with each other down to much lower temperatures ($T \sim 0.2$) in comparison to the bare sums. In addition, the last order (thick solid line) is in perfect agreement with the QMC results in the entire temperature region shown. Very similar results can be seen for the entropy in Fig. 6(b). Furthermore, as depicted in Fig. 6(c), and unlike the bare sums, the Wynn algorithm can precisely capture the position and the height of the peak in the specific heat of this model, and even converges to temperatures lower than those accessible to the QMC calculations depicted in the figure.

Note that the maximum cluster sizes considered in NLCE shown there (15 sites) are far smaller than the size of the lattice in the QMC simulations (256×265). Hence, we see that a thorough exploration of all topologies in NLCEs, up to those cluster sizes, completely eliminates finite-size effects. In addition, in combination with resummation algorithms, one can compute observables up to quite low temperatures. NLCE results can also be contrasted against those obtained from ED of a 16-site cluster with periodic boundary conditions. As seen in Fig. 6, the finite cluster results depart from QMC at temperatures higher than the convergence temperature of NLCE even with the bare sum. Using slightly larger clusters, which can still be solved by means of full exact diagonalization, does not improve this trend either [13].

We should point out that the AF Heisenberg model on the square lattice is one of the most challenging models that one can attempt to solve with NLCEs. This is because the antiferromagnetic correlations grow exponentially with decreasing temperature, and quickly exceed the linear size of the largest clusters that can be treated within ED. For this reason, frustrated magnetic systems,

for which QMC techniques run into the infamous sign problem, and where correlation lengths are small and grow slowly with decreasing temperature, are ideal to be explored by means of NLCEs.

Another very useful resummation technique for alternating series, i.e., series in which S_n alternates in sign, is the Euler transformation. Within this approach, S_n is replaced by $u_n = (-1)^n S_n$ and $P(\mathcal{L})/N$ is approximated by the following sum:

$$u_0 - u_1 + u_2 + \dots - u_{n-1} + \sum_{l=0}^{m-n} \frac{(-1)^l}{2^{l+1}} \Delta^l u_n, \quad (21)$$

where Δ is defined as forward differencing operator

$$\begin{aligned} \Delta^0 u_n &= u_n, \\ \Delta^1 u_n &= u_{n+1} - u_n, \\ \Delta^2 u_n &= u_{n+2} - 2u_{n+1} + u_n, \\ \Delta^3 u_n &= u_{n+3} - 3u_{n+2} + 3u_{n+1} - u_n, \\ &\vdots \end{aligned} \quad (22)$$

and $n - 1$ is the number of terms for which a bare sum is performed before the Euler transformation sets in for higher order terms. The first few terms of the approximation can be written as

$$P_m \rightarrow P_{n-1} + (-1)^n \left[\frac{1}{2} S_n + \frac{1}{4} (S_n + S_{n+1}) + \dots \right]. \quad (23)$$

It is evident from the results in Fig. 6 after implementing the Euler transformation for the last 11 terms ($n = 5$), that the latter algorithm also dramatically improves the convergence from that of the bare sum.

Acknowledgments

This research was supported by the National Science Foundation (NSF) under Grant No. OCI-0904597 and enabled by an allocation of advanced computing resources, supported by the NSF. The computations in Sec. 3 were performed on Kraken at the National Institute for Computational Science under Account No. TG-DMR100026.

References

- [1] C. Domb, M. S. Green, Phase Transitions and Critical Phenomena, Vol. 3, Academic Press, London, 1974.
- [2] H. C. Oitmaa, J., W. Zhang, Series Expansion Methods for Strongly Interacting Lattice Models, Cambridge University Press, Cambridge, England, 2006.
- [3] M. F. Sykes, J. W. Essam, B. R. Heap, B. J. Hiley, oLattice Constant Systems and Graph Theory, Journal of Mathematical Physics 7 (9) (1966) 1557–1572.

- [4] M. Rigol, T. Bryant, R. R. P. Singh, Numerical Linked-Cluster Approach to Quantum Lattice Models, *Phys. Rev. Lett.* 97 (18) (2006) 187202.
- [5] M. Rigol, T. Bryant, R. R. P. Singh, Numerical linked-cluster algorithms. I. Spin systems on square, triangular, and kagomé lattices, *Phys. Rev. E* 75 (6) (2007) 061118.
- [6] M. Rigol, T. Bryant, R. R. P. Singh, Numerical linked-cluster algorithms. II. $t - J$ models on the square lattice, *Phys. Rev. E* 75 (6) (2007) 061119.
- [7] R. R. P. Singh, J. Oitmaa, High-temperature series expansion study of the Heisenberg antiferromagnet on the hyperkagome lattice: Comparison with $\text{Na}_4\text{Ir}_3\text{O}_8$, *Phys. Rev. B* 85 (2012) 104406.
- [8] R. R. P. Singh, J. Oitmaa, Corrections to Pauling residual entropy and single tetrahedron based approximations for the pyrochlore lattice Ising antiferromagnet, *Phys. Rev. B* 85 (2012) 144414.
- [9] R. Applegate, N. R. Hayre, R. R. P. Singh, T. Lin, A. G. R. Day, M. J. P. Gingras, Is the $\text{Yb}_2\text{Ti}_2\text{O}_7$ pyrochlore a quantum spin ice?, *arXiv:1203.4569*.
- [10] E. Khatami, M. Rigol, Thermodynamics of strongly interacting fermions in two-dimensional optical lattices, *Phys. Rev. A* 84 (2011) 053611.
- [11] E. Khatami, M. Rigol, Effect of particle statistics in strongly correlated two-dimensional Hubbard models, *arXiv:1204.1556*.
- [12] B. Tang, T. Paiva, E. Khatami, M. Rigol, Short-Range Correlations and Cooling of Ultracold Fermions in the Honeycomb Lattice, *arXiv:1206.0006*.
- [13] E. Khatami, M. Rigol, Thermodynamics of the antiferromagnetic Heisenberg model on the checkerboard lattice, *Phys. Rev. B* 83 (2011) 134431.
- [14] E. Khatami, J. S. Helton, M. Rigol, Numerical study of the thermodynamics of clinoatcamite, *Phys. Rev. B* 85 (2012) 064401.
- [15] E. Khatami, R. R. P. Singh, M. Rigol, Thermodynamics and phase transitions for the Heisenberg model on the pinwheel distorted kagome lattice, *Phys. Rev. B* 84 (2011) 224411.
- [16] A. Irving, C. Hamer, Methods in hamiltonian lattice field theory (ii). linked-cluster expansions, *Nuclear Physics B* 230 (3) (1984) 361 – 384.
- [17] H. Y. Yang, K. P. Schmidt, Effective models for gapped phases of strongly correlated quantum lattice models, *EPL (Europhysics Letters)* 94 (1) (2011) 17004.
- [18] A. J. Guttmann, *Phase Transitions and Critical Phenomena*, Vol. 13, Academic Press, London, 1989.
- [19] H. W. Press, B. P. Flannery, S. A. Teukolsky, W. T. Vetterling, *Numerical Recipes in Fortran*, Cambridge University Press, Cambridge, England, 1999.